

Superior hardness and stiffness of diamond nanoparticles

Alexander Quandt ^a, Igor Popov ^b, David Tománek ^{c,*}

^a Mandelstam Institute for Theoretical Physics and School of Physics, University of the Witwatersrand, 2050, Johannesburg, South Africa

^b Institute of Physics Belgrade and Institute for Multidisciplinary Research, University of Belgrade, Belgrade, Serbia

^c Physics and Astronomy Department, Michigan State University, East Lansing, MI, 48824, USA

ARTICLE INFO

Article history:

Received 14 January 2020

Received in revised form

20 February 2020

Accepted 25 February 2020

Available online 29 February 2020

Keywords:

ab initio

Calculation

Stability

Hardness

Nanoparticle

DFT

ABSTRACT

We introduce a computational approach to estimate the hardness and stiffness of diamond surfaces and nanoparticles by studying their elastic response to atomic nanoindentation. Results of our *ab initio* density functional calculations explain the observed hardness differences between different diamond surfaces and suggest bond stiffening in bare and hydrogenated fragments of cubic diamond and lonsdaleite. The increase in hardness and stiffness can be traced back to bond length reduction especially in bare nanoscale diamond clusters, a result of compression that is driven by the dominant role of the surface tension.

© 2020 Elsevier Ltd. All rights reserved.

1. Introduction

In the field of ultrahard materials, the role of diamond as the hardest material on Earth seems to be well established. Not long ago, this fact has been disputed by reports that compressed fullerenes [1,2], nanotubes [3] and graphite [4–6], which occur as highly disordered and twinned nanocrystalline structures, may be still harder. Also crystalline C_3N_4 was initially believed to be harder than diamond due to its high bulk modulus [7], but ultimately turned out to be softer due to its inferior shear modulus [8,9]. On the macro-scale, mechanical hardness is commonly associated with plastic deformations introduced by an external force, whereas mechanical stiffness is associated with resistance to compression and shear in the elastic regime. This distinction becomes blurred on the nanometer scale, where the energy cost of introducing plastic deformations exceeds that of fracture [10]. There, a scratch test appears to be a more suitable measure of hardness, since the harder system need not undergo irreversible plastic deformations.

So far, theoretical attempts to correlate mechanical hardness with a particular bulk crystal structure have been mostly disappointing [11–18]. More recently, theoretical and experimental

studies have established a correlation between hardness, stiffness, and linear elastic constants in covalently bounded materials [19–21]. A new interesting evidence suggests that indentation hardness may be proportional to the gravimetric density in carbon materials [22]. Progress in computational materials science suggests that *ab initio* calculations should be a valuable approach to determine the stiffness and hardness of systems beyond the reach of common experimental techniques. Observations in polycrystalline materials including cubic boron nitride indicate an increasing hardness with decreasing size of the nanocrystallites [23,24]. We find it conceivable that also diamond nanoparticles [25] should be harder than their macroscopic counterparts due to the dominant role of the surface tension, which compresses the nanoparticles and stiffens the interatomic interactions in the anharmonic regime. In the macro-scale counterpart, stiffening of diamond under pressure is evidenced in the non-vanishing third-order elastic constants [26].

At this point, we must emphasize that dislocation defects are absent in nanosized particles due to the associated large energy penalty. Consequently, Hall-Petch strengthening [27,28] associated with dislocation motion does not occur in nanoparticles. This fact sets nanostructures apart from their bulk counterparts.

Here we introduce a computational approach to estimate and compare the hardness and stiffness of diamond surfaces and nanoparticles, independent of size, by studying their elastic

* Corresponding author.

E-mail address: tomanek@msu.edu (D. Tománek).

response to atomic nanoindentation. Results of our *ab initio* density functional calculations explain the observed stiffness differences between different diamond surfaces and indicate the occurrence of bond stiffening in bare and hydrogenated fragments of cubic diamond and of lonsdaleite. The increase in stiffness, especially in bare diamond fragments, can be traced back to bond length reduction that is driven by compression and caused by the surface tension. In absence of plastic deformations on the nanometer scale, increased stiffness corresponds to an increase in hardness.

2. Results

The relaxed geometries of hydrogen-terminated C_nH_m diamondoid nanoparticles with $10 \leq n \leq 136$ carbon atoms, obtained as fragments of cubic diamond and lonsdaleite, also called hexagonal diamond, are shown in Fig. 1. Since all carbon atoms are sp^3 -hybridized in these hydrogen terminated systems, the equilibrium atomic arrangement is very close to that in the bulk structure. The situation is very different in bare carbon nanoparticles, where a significant fraction of surface atoms with unsaturated bonds causes large-scale reconstruction of the structures. The equilibrium structure of C_n nanoparticles [29] comprises sp^1 -bonded chains

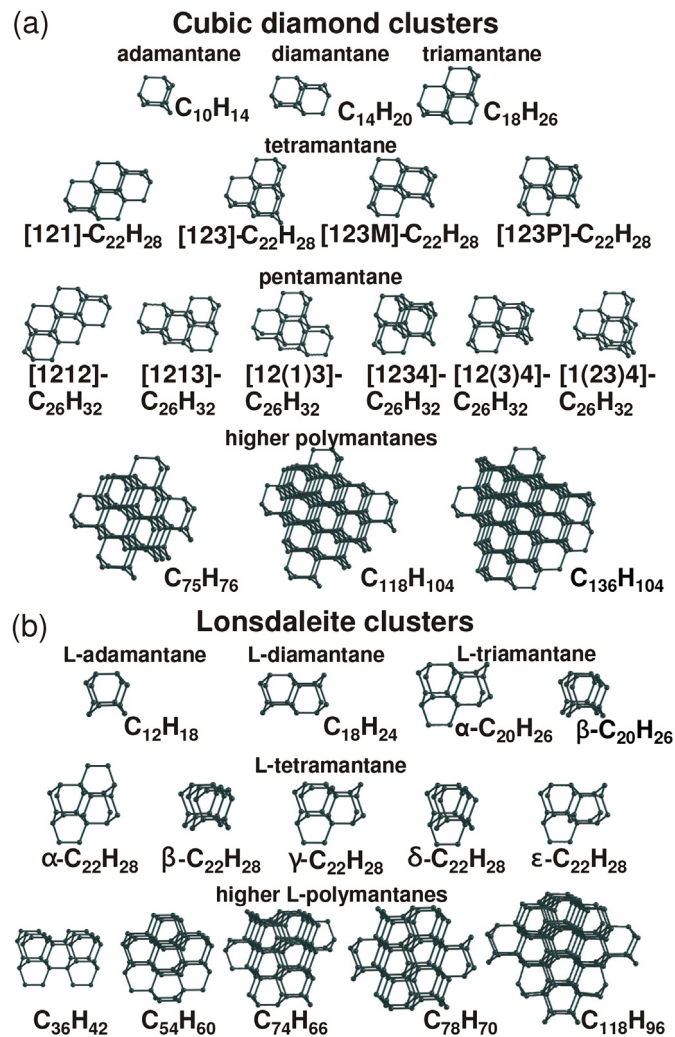


Fig. 1. Ball-and-stick models of (a) cubic diamond and (b) lonsdaleite nanoparticles. Terminating hydrogen atoms have been omitted for clarity. (A colour version of this figure can be viewed online.)

and rings for $n < 20$ and sp^2 -bonded fullerenes for $n \geq 20$. Some small nanoparticles, including the C_{10} adamantane and C_{14} diamantane, maintain their strained diamond-like morphology as metastable structures. We found all larger nanoparticles in this study, with diameters up to ≈ 7 Å, to be unstable with respect to surface graphitization due to the dominant role of unsaturated bonds at the surface. This is true even in very large nanoparticles such as C_{136} , where half the atoms change their hybridization from sp^3 to sp^2 .

As mentioned in the Introduction, mechanical hardness H is commonly associated with resilience to plastic deformations introduced by an external force. In macroscopic structures, H is measured by nanoindentation and defined by the ratio of the load acting on a sharp nanoindenter and the resulting indentation depth, as indicated schematically in Fig. 2 (a). It is an integral characteristic of a solid that reflects resistance to compression and shear and depends on quantities such as ductility, elastic stiffness, plasticity, strength, toughness, and viscosity. Since this complex response is hard to reproduce by *ab initio* techniques, a number of empirical approaches have been developed in recent years to estimate this quantity [31]. Model calculations [32,33], which have relied on simplified expressions based on a combination of valence charges, bond ionicities and interatomic distances, have so far failed to describe the dependence of hardness on the surface orientation in extended solids. Due to their dependence on a suitable choice of parameters, such model approaches are typically limited to a specific class of systems.

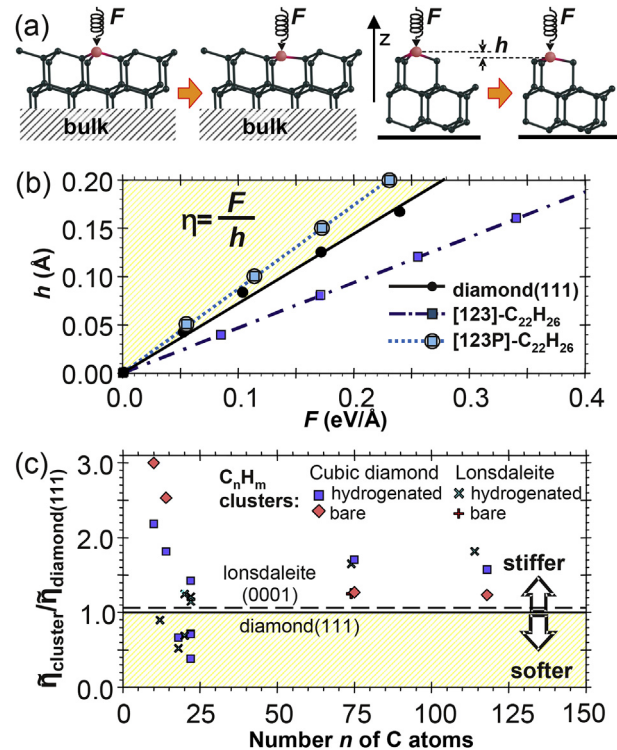


Fig. 2. (a) Schematic of an atomic nanoindenter. The displacement h of a surface atom, highlighted in red, after being subject to force F , serves as a local probe of hardness and stiffness of crystal surfaces and nanoparticles. Bulk atoms far underneath the extended surface and at the bottom of nanoparticles are constrained in the direction of the force. (b) Calculated $F-h$ relationship at the (111) cubic diamond surface and in two tetramantane isomers. (c) Normalized hardness η in bare and hydrogen terminated nanoparticles of cubic diamond and lonsdaleite compared to the corresponding quantity for the (111) surface of cubic diamond. Shaded regions in (b) and (c) represent response in systems softer than diamond. (A colour version of this figure can be viewed online.)

In principle, direct calculations of indentation [30] should be able to describe hardness anisotropy. Such studies would, however, necessitate very large unit cells that currently exceed the scope of accurate *ab initio* calculations. Here we introduce an alternative way to predict differences in hardness based on the elastic response to particular deformations that is based on *ab initio* total energy calculations. We have considered specifically the Rockwell nano-indentation technique [34], which relates hardness to the indentation depth caused by a conical nanoindenter that is rammed into a surface by a given force. To extend our results to nanoparticles, which are much smaller than any nanoindenter, we have identified an individual surface atom as a nanoindenter. Then, we relate the local hardness and stiffness to the $\eta = F/h$ ratio of the normal force F to the atomic displacement h .

This approach naturally describes the response to compression and shear on the atomic scale and allows us to discriminate between different surface orientations. The atomic nanoindenter is shown schematically in Fig. 2(a) for semiinfinite surfaces and nanoparticles. Our calculations determine directly the chemical stiffness of interatomic bonds at the diamond surface. This quantity is related to the earlier-defined chemical hardness [34], which measures the resistance to a change in chemical bonding. As demonstrated earlier [35], the indentation hardness is a monotonic function of the chemical hardness density.

In our computational nanoindentation study, with a setup depicted in Fig. 2(a), we displace a particular atom by the distance h normal to the surface, relax the system, and determine the force acting on the nanoindenter atom from $F = -\partial E_{total}/\partial h$. This approach requires specific structural constraints, which we specify in Section 5 on Computational Techniques.

For indentation depths h not exceeding a fraction of the carbon-carbon bond length d_{CC} , we find a linear relationship between h and F , as seen in our results for the (111) surface of cubic diamond and two tetramantane isomers in Fig. 2(b). Our results indicate that the force constant η of the [123] diamond isomer is larger and that of the [123P] isomer is lower than that of the (111) surface of cubic diamond. We conclude that the hardness of these particular diamond fragments is close to, and may even exceed that of the bulk crystalline diamond structure.

To compare the hardness of different crystal surfaces, we introduce the normalized hardness $\tilde{\eta}$, which we define by

$$\tilde{\eta} = \frac{\eta}{A} = \frac{F}{h \cdot A}, \quad (1)$$

where A is the area per atom at a particular surface. We have combined observed hardness values H with our calculated values of the related quantity $\tilde{\eta}$ for different surfaces of cubic diamond and lonsdaleite in Table 1. Experimental data indicate that the (111) surface is the hardest surface of cubic diamond and that the (100) surface is 18% softer. Even though our computational approach does not provide absolute hardness values, the calculated ratio $\tilde{\eta}(100)/$

$\tilde{\eta}(111) = 0.88$ agrees well with the ratio of the observed hardness values $H(100)/H(111) = 0.82$ in cubic diamond [1]. There are no experimental observations for the lonsdaleite structure, which occurs only as inclusions in cubic diamond and is believed to be somewhat harder. Based on our calculated values of $\tilde{\eta}$ listed in Table 1, we believe that the (0001) surface of lonsdaleite may be 2% harder than the (111) surface of cubic diamond.

Results in Table 1 indicate that presence of lonsdaleite alone may not explain reported hardness values that are significantly higher than those of cubic diamond [1-6]. Therefore, we determine the normalized hardness $\tilde{\eta}$ also for hydrogen-terminated and bare diamond nanoparticles. For a reasonable comparison, we have aligned each nanoparticle so that the topmost atom of the unrelaxed structure, which will be subject to force F , belongs to the (111) surface of cubic diamond or to the corresponding (0001) surface of lonsdaleite. Since the area per atom is affected by the net contraction of the nanoparticle, we estimated its surface area S from that of a polyhedron spanned by the nuclei of the outermost atoms. We then used $A = A_i \times (S_f/S_i)$ for the atom area in Eq. (1), where A_i is the area per atom at the corresponding infinite surface and S_f/S_i is the ratio of total nanoparticle surface areas in the final (f) and the initial (i) structures.

We present our results for $\tilde{\eta}$ in hydrogen covered and bare nanoparticles of cubic diamond as well as lonsdaleite in Fig. 2(c) and compare them to those for the (111) surface of cubic diamond. Our results indicate that a significant fraction of diamond nanoparticles appears to be significantly harder than the hardest diamond surface. We find large differences in the calculated values of $\tilde{\eta}$ even between different isomers of the same nanostructure, such as the [123] and [123P] isomers of tetramantane. Their different elastic response, depicted in Fig. 2(b), reflects the simple fact that particular structures may expand more or less easily in the plane normal to the applied force. This flexibility is partly suppressed in polycrystalline bulk assemblies of nanoparticles and also in larger free-standing structures, which, however, approach bulk diamond values with increasing nanoparticle size.

3. Discussion

There is an intuitive explanation for our finding that the apparent hardness increases with decreasing size of diamond nanoparticles. We need to note at this point that hardness enhancement in nanoparticles of diamond and other solids is fundamentally different from the behavior observed in macrostructures, often described as the Hall-Petch effect, which is associated with the nucleation and motion of dislocations [27,28]. As mentioned earlier, plastic deformations do not occur in nanoparticles due to the associated high energy cost.

In nanoparticles with a significant portion of surface atoms, surface tension reduces significantly the surface area and thus the interatomic bond length d_{CC} . We have determined the bond length distribution in all nanoparticles presented in Fig. 1 and plot this quantity separately for bare and for hydrogenated nanoparticles in Fig. 3(a). Termination by hydrogen reduces the surface energy and provides a bulk-like bonding environment even for carbon atoms at the surface. Therefore, bond lengths in hydrogenated nanoparticles are all close to the 1.54 Å value found in sp^3 -hybridized diamond. On the other hand, we observe a significant bond length contraction in bare diamond nanoparticles. Under-coordinated atoms at the surface, which dominate in small nanoparticles, reconstruct to form a “net” that contains and compresses the “bulk” of the structure in a “snug fit”. Most surface atoms relax to a more favorable sp^2 -like graphitic bonding geometry with $d_{CC} \approx 1.42$ Å. Only a small fraction of two-fold coordinated surface atoms is bonded in an sp^1 -like carbyne environment with $d_{CC} \approx 1.28$ Å. The

Table 1

Observed hardness H and calculated normalized hardness $\tilde{\eta}$ at the (111) and (100) surfaces of cubic diamond and the (0001) surface of lonsdaleite, as well as ratios of these quantities.

	Diamond		(100)	Lonsdaleite	(0001)
	(111)	(100)	(111)	(0001)	(111)
H (GPa)	167±5 ^a	137±6 ^a	0.82±0.06	–	–
$\tilde{\eta}$ (eV/Å ³)	117 ^b	95 ^b	0.81	0.74	1.02

^a Ref. [1].

^b Ref. [30].

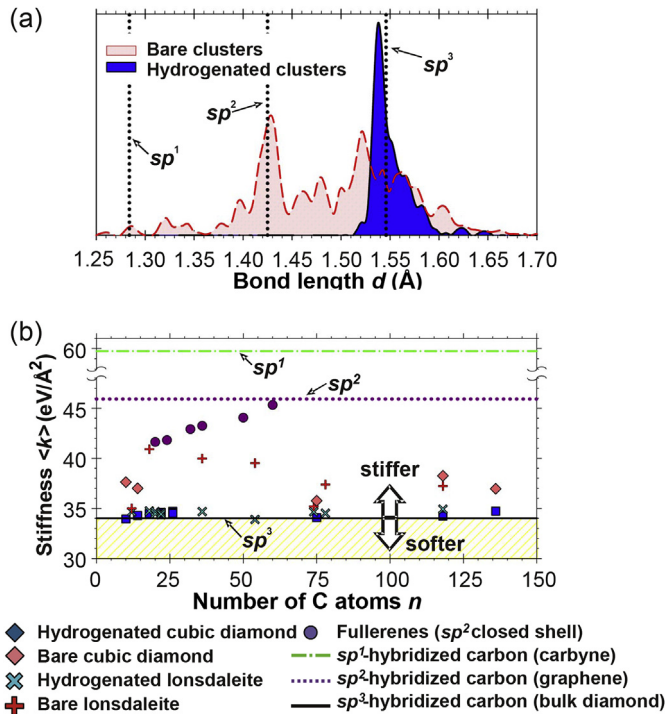


Fig. 3. (a) Bond length distribution in C_nH_m diamond nanoparticles of Fig. 1. The light (red) shaded area below the dashed line represents bare C_n nanoparticles, and the dark (blue) shaded area below the solid line represents hydrogenated nanoparticles. (b) Comparison between the average bond stiffness $\langle k \rangle$, defined in Eq. (2), in the nanoparticles of panel (a) and in sp^1 , sp^2 and sp^3 bonded bulk systems. (A colour version of this figure can be viewed online.)

degree of bond contraction we find in nano-diamond agrees with estimates for nanometer-sized diamond particles based on elastic constants and surface energy. Due to the anharmonicity in the interatomic bonds, the net bond contraction should cause a stiffening in particular of bare nanoparticles. This reasoning is consistent with the recent observation [22] that indentation hardness increases at higher densities caused by bond contraction and reconstruction in nanostructures.

To validate our interpretation, we estimated the bond stiffness in nanoparticles considered in our study. In each optimized nanoparticle, we first determined the average bond length $\langle d_{CC,0} \rangle$ and the bond energy $E_{b,0} = E_{coh,0}/N_b$ by dividing the cohesive energy E_{coh} by the number of nearest-neighbor bonds N_b . We then uniformly expanded or contracted the nanoparticle and determined the corresponding average bond length $\langle d_{CC,0} \rangle$ and bond energy E_b . Finally, we determined the average bond stiffness $\langle k \rangle$ in a given particle using

$$|E_b - E_{b,0}| = \frac{1}{2} \langle k \rangle (\langle d_{CC} \rangle - \langle d_{CC,0} \rangle)^2. \quad (2)$$

We plot the quantity $\langle k \rangle$ for C_nH_m nanoparticles and compare it to that of sp^3 , sp^2 and sp^1 hybridized systems in Fig. 3(b). Our results indicate that the bond stiffness in hydrogenated nanoparticles is comparable to that in sp^3 -hybridized diamond and is typically much higher in bare nanoparticles, approaching the higher bond stiffness of sp^2 -hybridized graphene. For the sake of fair comparison, we also present bond stiffness values of fullerenes in Fig. 3(b). These hollow graphitic nanoparticles display sp^2 bonding with a small sp^3 admixture, and their bond stiffness values are in the expected range. We conclude that the enhanced bond stiffness in bare nanoparticles is caused by surface reconstruction from

dominant sp^3 to at least partial sp^2 -type bonding. We may expect that diamond nanoparticles with a graphitized outer surface, which are often observed experimentally [36], may have stiffer bonds than diamond.

At this point we should re-emphasize that the connection between bond stiffness, reflecting elastic response, and hardness, which describes irreversible plastic deformations, is only indirect. Bond stiffness describes the resistance of bonds to stretching and compression, which we model by uniformly compressing the entire structure. On the other hand, hardness characterizes the resistance of a structure to indentation, which we model by displacing one single surface atom. The hardest nanoparticles in our study were bare and hydrogen-terminated $C_{10}H_x$ adamantane and $C_{14}H_x$ diamantane nanoparticles. With the exception of these two systems, hydrogenated nanoparticles were found to be harder than bare nanoparticles. The significant increase in nominal hardness, which we found in ultra-small nanoparticles, diminishes rapidly in systems containing hundreds of carbon atoms and approach rapidly well-established bulk values.

4. Summary and conclusions

In conclusion, we have introduced a computational approach to estimate and compare the hardness and stiffness of both single-crystal surfaces and nanoparticles of diamond, which are too small for indentation experiments, by studying their elastic response to atomic nanoindentation. Results of our *ab initio* density functional calculations of this nanoindentation process correlated well with the observed differences in hardness between different diamond surfaces. More important, we find bond stiffening in bare and hydrogenated fragments of both cubic diamond and lonsdaleite. The increase in stiffness, especially in bare nano-diamond particles, can be traced back to bond length reduction. The net average bond compression is driven by the dominant role of the surface tension and leads to surface reconstruction. Since plastic deformations do not occur on the nanometer scale, increased stiffness indicates an increase in hardness. It is likely that the scratch hardness of diamond nanoparticles, which are used to cover drill heads, may exceed that of monocrystalline diamond.

5. Computational Techniques

5.1. Representation of nanoindentation

We represent a periodic infinite surface, shown in the left panels of Fig. 2(a), by a unit cell with a finite surface area, which contains infinitely many atoms below the surface. In principle, the displacement of the atomic nanoindenter along the $-z$ direction into the surface may cause all atoms within the unit cell to move, but the shape of the unit cell will not change. In our study, we only allow atomic displacement within a thick surface region above a frozen bulk structure that balances the force caused by the nanoindenter. E_{total} is determined for the optimized geometry.

In finite nanoparticles, depicted in the right panels of Fig. 2(a), there are no symmetry restrictions on atomic displacements or global shape deformations. To provide a realistic description of nanoindentation in a previously relaxed nanoparticle, we first displace the atomic nanoindenter along the $-z$ direction. Next, we fix the z -coordinates, but not the x - and y -coordinates, of all bottom atoms of the nanoparticle to balance the force caused by the nanoindenter. Finally, we relax all remaining atomic degrees of freedom and determine E_{total} . For both infinite surfaces and finite nanoparticles, we obtain the force that caused the deformation from $F = -\partial E_{total}/\partial h$.

5.2. Total energy formalism

Our calculations of the optimum atomic structure, stability and elastic properties of diamond surfaces and nanoparticles are based on the density functional theory (DFT) [37,38]. We used the PBE-PAW approximation [39] to DFT, as implemented in the VASP [40–42] code. All systems have been represented using periodic boundary conditions and a plane-wave energy cutoff of 520 eV. Spurious interaction between neighboring particles has been suppressed by requiring the closest-approach distance between adjacent surfaces to exceed [43] 6 Å. All structures have been relaxed until all forces acting on atoms were less than 0.01 eV/Å.

Declaration of competing interest

The authors declare that they have no known competing financial interests or personal relationships that could have appeared to influence the work reported in this paper.

CRedit authorship contribution statement

Alexander Quandt: Methodology, Validation, Writing - original draft. **Igor Popov:** Investigation, Visualization, Writing - original draft. **David Tománek:** Conceptualization, Methodology, Visualization, Validation, Writing - original draft.

Acknowledgments

We thank Mikhail Yu. Popov and Arthur G. Every for useful discussions. This study was supported by the NSF/AFOSR EFRI 2-DARE grant number EFMA-1433459. Computations have been performed by Liubov Yu. Antipina and Pavel B. Sorokin while visiting Michigan State University in 2013–2014. Computational resources have been provided by the Michigan State University High Performance Computing Center and the Moscow State University Supercomputer. AQ thanks the Materials for Energy Research Group (MERG) and the DST-NRF Centre of Excellence in Strong Materials (CoE-SM) at the University of the Witwatersrand for support. AQ and DT also thank the Mandelstam Institute for Theoretical Physics (MITP) and the Simons Foundation, award number 509116, for support.

References

- [1] V. Blank, M. Popov, G. Pivovarov, N. Lvova, K. Gogolinsky, V. Reshetov, Ultrahard and superhard phases of fullerite C₆₀: comparison with diamond on hardness and wear, *Diam. Relat. Mater.* 7 (2–5) (1998) 427–431.
- [2] L. Wang, B. Liu, H. Li, W. Yang, Y. Ding, S.V. Sinogeikin, Y. Meng, Z. Liu, X.C. Zeng, W.L. Mao, Long-range ordered carbon clusters: a crystalline material with amorphous building blocks, *Science* 337 (6096) (2012) 825–828.
- [3] M. Popov, M. Kyotani, Y. Koga, Superhard phase of single-wall carbon nanotube, *Phys. B Condens. Matter* 323 (1–4) (2002) 262–264.
- [4] W.L. Mao, H. Mao, P.J. Eng, T.P. Trainor, M. Newville, C. Kao, D.L. Heinz, J. Shu, Y. Meng, R.J. Hemley, Bonding changes in compressed superhard graphite, *Science* 302 (5644) (2003) 425–427.
- [5] T. Irifune, A. Kurio, S. Sakamoto, T. Inoue, H. Sumiya, Ultrahard polycrystalline diamond from graphite, *Nature* 421 (2003) 599–600.
- [6] K. Tanigaki, H. Ogi, H. Sumiya, K. Kusakabe, N. Nakamura, M. Hirao, H. Ledbetter, Observation of higher stiffness in nanopolycrystal diamond than monocrystal diamond, *Nat. Commun.* 4 (2013) 2343.
- [7] A.Y. Liu, M.L. Cohen, Prediction of new low compressibility solids, *Science* 245 (4920) (1989) 841–842.
- [8] D.M. Teter, R.J. Hemley, Low-compressibility carbon nitrides, *Science* 271 (5245) (1996) 53–55.
- [9] G.S. Manyali, R. Warmbier, A. Quandt, J.E. Lowther, *Ab initio* study of elastic properties of super hard and graphitic structures of C₃N₄, *Comput. Mater. Sci.* 69 (2013) 299–303.
- [10] A. Griffith, VI. The phenomena of rupture and flow in solids, *Phil. Trans. Roy. Soc. Lond.* A221 (1920) 163–198.
- [11] L. Chernozatonskii, N. Serebryanaya, B. Mavrin, The superhard crystalline three-dimensional polymerized C₆₀ phase, *Chem. Phys. Lett.* 316 (3–4) (2000) 199.
- [12] S. Berber, E. Osawa, D. Tomanek, Rigid crystalline phases of polymerized fullerenes, *Phys. Rev. B* 70 (8) (2004) 085417.
- [13] Q. Li, Y. Ma, A.R. Oganov, H. Wang, H. Wang, Y. Xu, T. Cui, H.-K. Mao, G. Zou, Superhard monoclinic polymorph of carbon, *Phys. Rev. Lett.* 102 (17) (2009) 175506.
- [14] K. Umemoto, R.M. Wentzcovitch, S. Saito, T. Miyake, Body-centered tetragonal C⁴: sp³carbon allotrope, *Phys. Rev. Lett.* 104 (12) (2010) 125504.
- [15] J.-T. Wang, C. Chen, Y. Kawazoe, Low-temperature phase transformation from graphite to sp³orthorhombic carbon, *Phys. Rev. Lett.* 106 (7) (2011), 075501.
- [16] D. Selli, I.A. Baburin, R. Martoňák, S. Leoni, Superhard sp³carbon allotropes with odd and even ring topologies, *Phys. Rev. B* 84 (2011) 161411.
- [17] M. Amsler, J.A. Flores-Livas, L. Lehtovaara, F. Balima, S.A. Ghasemi, D. Machon, S. Pailhès, A. Willand, D. Caliste, S. Botti, A. San Miguel, S. Goedecker, M.A.L. Marques, Crystal structure of cold compressed graphite, *Phys. Rev. Lett.* 108 (2012), 065501.
- [18] Y.A. Kvashnina, A.G. Kvashnin, P.B. Sorokin, Investigation of new superhard carbon allotropes with promising electronic properties, *J. Appl. Phys.* 114 (18) (2013) 183708.
- [19] X.-Q. Chen, H. Niu, D. Li, Y. Li, Modeling hardness of polycrystalline materials and bulk metallic glasses, *Intermetallics* 19 (9) (2011) 1275–1281.
- [20] V.A. Mukhanov, O.O. Kurakevych, V.L. Solozhenko, Thermodynamic aspects of materials' hardness: prediction of novel superhard high-pressure phases, *High Pres. Res.* 28 (4) (2008) 531–537.
- [21] X. Jiang, J. Zhao, X. Jiang, Correlation between hardness and elastic moduli of the covalent crystals, *Comput. Mater. Sci.* 50 (7) (2011) 2287–2290.
- [22] S. Kang, Z. Xiang, H. Mu, Y. Cai, Mechanical properties, lattice thermal conductivity, infrared and Raman spectrum of the fullerite C₂₄, *Phys. Lett. A* 384 (1) (2020) 126035.
- [23] N. Dubrovinskaia, V.L. Solozhenko, N. Miyajima, V. Dmitriev, O.O. Kurakevych, L. Dubrovinsky, Superhard nanocomposite of dense polymorphs of boron nitride: noncarbon material has reached diamond hardness, *Appl. Phys. Lett.* 90 (10) (2007) 101912.
- [24] V.L. Solozhenko, O.O. Kurakevych, Y.L. Godec, Creation of nanostructures by extreme conditions high-pressure synthesis of ultrahard nanocrystalline cubic boron nitride, *Adv. Mater.* 24 (12) (2012) 1540–1544.
- [25] J.E. Dahl, J.M. Moldovan, K.E. Peters, G.E. Claypool, M.A. Rooney, G.E. Michael, M.R. Mello, M.L. Kohnen, Diamondoid hydrocarbons as indicators of natural oil cracking, *Nature* 399 (7) (1999) 54–57.
- [26] M.H. Grimsditch, E. Anastassakis, M. Cardona, Effect of uniaxial stress on the zone-center optical phonon of diamond, *Phys. Rev. B* 18 (1978) 901–904.
- [27] H. Van Swygenhoven, Grain boundaries and dislocations, *Science* 296 (5565) (2002) 66–67.
- [28] Y. Mo, D. Stone, I. Szlufarska, Strength of ultrananocrystalline diamond controlled by friction of buried interfaces, *J. Phys. D Appl. Phys.* 44 (40) (2011) 405401, and 45, 069501 (2012) (E).
- [29] D. Tomanek, M.A. Schluter, Growth regimes of carbon clusters, *Phys. Rev. Lett.* 67 (17) (1991) 2331–2334.
- [30] A. Richter, R. Ries, R. Smith, M. Henkel, B. Wolf, Nanoindentation of diamond, graphite and fullerene films, *Diam. Relat. Mater.* 9 (2) (2000) 170–184.
- [31] Y. Tian, B. Xu, Z. Zhao, Microscopic theory of hardness and design of novel superhard crystals, *Int. J. Refract. Metals Hard Mater.* 33 (2012) 93–106.
- [32] A. Šimůnek, Anisotropy of hardness from first principles: the cases of ReB₂ and OsB₂, *Phys. Rev. B* 80 (2009), 060103.
- [33] F. Gao, Theoretical model of hardness anisotropy in brittle materials, *J. Appl. Phys.* 112 (2) (2012), 023506.
- [34] J. Gilman, *Chemistry and Physics of Mechanical Hardness*, John Wiley & Sons, 2009.
- [35] W. Yang, R.G. Parr, L. Uytterhoeven, New relation between hardness and compressibility of minerals, *Phys. Chem. Miner.* 15 (2) (1987) 191–195.
- [36] S. Welz, Y. Gogotsi, M.J. McNallan, Nucleation, growth, and graphitization of diamond nanocrystals during chlorination of carbides, *J. Appl. Phys.* 93 (7) (2003) 4207.
- [37] P. Hohenberg, W. Kohn, Inhomogeneous electron gas, *Phys. Rev.* 136 (3B) (1964) 864–871.
- [38] W. Kohn, L.J. Sham, Self-consistent equations including exchange and correlation effects, *Phys. Rev.* 140 (4A) (1965) 1133–1138.
- [39] J.P. Perdew, K. Burke, M. Ernzerhof, Generalized gradient approximation made simple, *Phys. Rev. Lett.* 77 (18) (1996) 3865–3868.
- [40] G. Kresse, J. Hafner, *Ab initio* molecular dynamics for liquid metals, *Phys. Rev. B* 47 (1) (1993) 558–561.
- [41] G. Kresse, J. Hafner, *Ab initio* molecular-dynamics simulation of the liquid-metal-amorphous-semiconductor transition in germanium, *Phys. Rev. B* 49 (20) (1994) 14251–14269.
- [42] G. Kresse, J. Furthmüller, Efficient iterative schemes for *ab initio* total-energy calculations using a plane-wave basis set, *Phys. Rev. B* 54 (1996) 11169–11186.
- [43] On a per-surface-atom basis, the interaction energy between diamond surfaces separated by 6 Å differs by less than 0.02 meV from that for surfaces separated by 10 Å.